Renewable Energy 256 (2026) 124424

Contents lists available at ScienceDirect

Renewable Energy

journal homepage: www.elsevier.com/locate/renene

Gasification of Malaysian agricultural and industrial biomass in CO_2: A physicochemical characterization and thermogravimetric-based ranking approach

Zi Wei Ng [a], Arshad Adam Salema [a,b,*], Izzudin Ibrahim [c], Hazratul Mumtaz Lahuri [d], Yi Herng Chan [d]

[a] Sustainable Energy and Development Lab, Department of Mechanical Engineering, School of Engineering, Monash University Malaysia, Jalan Lagoon Selatan, 47500, Bandar Sunway, Selangor, Malaysia
[b] Centre for Net-Zero Technology (CNZT), School of Engineering, Monash University Malaysia, Jalan Lagoon Selatan, 47500, Bandar Sunway, Selangor, Malaysia
[c] Department of Chemical and Environmental Engineering, Faculty of Engineering, Universiti Putra Malaysia, Serdang, 43400, Selangor, Malaysia
[d] PETRONAS Research Sdn. Bhd. (PRSB), Lot 3288 & 3289, off Jalan Ayer Itam, Kawasan Institusi Bangi, 43000, Kajang, Selangor, Malaysia

ARTICLE INFO

Keywords:
Biomass
Ranking
CO_2
Gasification
Kinetic
Catalyst

ABSTRACT

Currently, industries capture and store carbon dioxide (CO_2), but they are seeking a long-term solution to convert the captured CO_2 into value-added products. The main aim of this study is to rank the Malaysian agricultural and industrial biomasses: empty fruit bunches (EFB), palm kernel shell (PKS), sawdust (SD), rice husk (RH), and coconut shell (CS) based on physicochemical properties, kinetic, thermodynamic parameters, and their interaction with CO_2 (gasifying agent), utilizing thermogravimetric analysis (TGA). Gasification proceeded via a two-stage thermal degradation process: pyrolysis (below 380 °C - I) and char gasification (beyond 380 °C - II). Kinetic analysis revealed a catalyst-induced reduction in activation energy during Stage II. Thermodynamic analysis showed positive enthalpy change (ΔH) exhibited endothermic reaction requirements, while positive Gibbs free energy change (ΔG) indicated a non-spontaneous process. EFB emerged as the top-ranked biomass (EFB > PKS > CS > SD > RH) based on integrated characterization, kinetic, and thermodynamic outcomes. The application of dolomite and olivine catalysts significantly enhanced gasification kinetics, particularly for EFB and RH, by reducing ΔH. The biomass ranking framework will benefit researchers and industries to prioritize biomass feedstock based on their performance, paving the way for the practical implementation in CO_2 gasification.

Nomenclature:

Symbols	Abbreviation
CO_2	Carbon dioxide
ΔG	Change in Gibbs free energy
ΔH	Change in Enthalpy
ΔS	Change in Entropy
EFB	Empty fruit bunch
PKS	Palm kernel shell
SD	Sawdust
RH	Rice husk
CS	Coconut shell
MC	Moisture content
VM	Volatile matter
FC	Fixed carbon
TGA	Thermogravimetric analysis
LAP	Laboratory Analytical Procedure
NREL	National Renewable Energy Laboratory
XRF	X-Ray Fluorescence
XRD	X-ray powder diffraction
FTIR	Fourier transform infrared
TG	Thermogravimetry
DTG	Derivative thermogravimetric
FWO	Flynn-Wall-Ozawa
STK	Starink
KAS	Kissinger-Akahira-Sunose
E_a	Activation energy
$m_{biomass}$	Weight of biomass
ΔT	Temperature difference

(continued on next column)

(continued)

(continued on next page)

* Corresponding author. Sustainable Energy and Development Lab, Department of Mechanical Engineering, School of Engineering, Monash University Malaysia, Jalan Lagoon Selatan, 47500, Bandar Sunway, Selangor, Malaysia.
E-mail address: arshad.salema@monash.edu (A.A. Salema).

https://doi.org/10.1016/j.renene.2025.124424
Received 3 May 2025; Received in revised form 8 August 2025; Accepted 16 September 2025
Available online 20 September 2025

(*continued*)

CrI	Segal crystallinity index
I_{200}	Crystalline peak
I_{am}	Amorphous peak intensity value
β	Heating rate
A	Pre-exponential factor
R	Ideal gas constant
T_m	Temperature of the maximum peak observed in the DTG curve
k_B	Boltzmann constant
h	Plank constant

1. Introduction

Achieving net-zero emissions by 2050 has become a crucial goal in combating climate change and transitioning toward a sustainable and resilient future [1]. This transition demands the urgent adoption of innovative and sustainable technologies to address the heavy reliance on fossil-derived energy and the associated environmental consequences, particularly the excessive release of carbon dioxide (CO_2). Industries have increasingly adopted carbon capture, utilization, and storage (CCUS) technologies to reduce greenhouse gas emissions and avoid carbon taxes. However, they are looking for long-term solutions to convert captured CO_2 into useable and marketable products. Conversely, renewable technologies have gained significant attention to curb carbon emissions. For instance, biomass is a carbon-neutral resource with immense potential to mitigate environmental challenges.

Malaysia generates significant agricultural and industrial biomass annually, offering valuable feedstocks for sustainable energy applications. The primary types of biomass generated include empty fruit bunches (EFB, *Elaeis Guineensis*), palm kernel shell (PKS, *Elaeis Guineensis*), sawdust (SD, *Neobalanocarpus Heimii*, *Hevea Brasiliensis*, *Tectona Grandis*), rice husk (RH, *Oryza Sativa*), and coconut shell (CS, *Cocos Nucifera*) [2]. In 2022, palm oil mills in Malaysia produced approximately 20 million tonnes of EFB and 5.2 million tonnes of PKS, while agricultural and forestry activities yielded 2 million tonnes of sawdust, 0.5 million tonnes of rice husk, and 0.1 million tonnes of coconut shells [3]. Current practices include the direct combustion of EFB and PKS for bioenergy generation [4], the use of rice husk and sawdust in composite material manufacturing and as fuel for brick kilns [5,6], and the processing of coconut shells into activated carbon or traditional cooking fuel [7]. However, their potential to be converted into high-value-added products, using alternative thermochemical processes such as gasification, is not fully explored.

Gasification, a well-established thermochemical process, offers a transformative pathway by converting biomass into syngas (a mixture of hydrogen and carbon monoxide) that can be further processed into value-added chemicals and fuels [8,9]. This aligns with industry goals to integrate CO_2 utilization into gasification processes, creating sustainable and economically viable products such as biofuels and sustainable aviation fuels. Recently, there has been growing interest in using CO_2 as a gasifying agent to eliminate carbon emissions and enhance the gasification product. CO_2 gasification produces syngas with the potential for chemical production with a specific CO-to-H_2 ratio and reduces the nitrogen content (if air is replaced with CO_2 as a gasifying agent) in syngas, minimizing undesirable by-products [10]. Fundamental knowledge of biomass thermal behavior and kinetics in a CO_2 environment is critical before scaling up the process.

Recent advances in understanding the biomass gasification mechanism in a CO_2 environment, using thermogravimetric analysis (TGA), have provided significant insights into this process. Prabhakar et al. [11] employed TGA to study the gasification behavior of coal char in a CO_2 environment and concluded that CO_2 gasification is an endothermic process. Wang et al. [12] conducted a kinetic study of CO_2-corn straw gasification using TGA combined with Fourier Transform Infrared Spectroscopy (FTIR), identifying the distinct stages of pyrolysis and biochar gasification while determining activation energies for each stage. Their findings revealed the complexity of biomass structures and their influence on gasification mechanisms. Pacioni et al. [13] examined the CO_2 gasification behavior of biochar derived from Brazilian agro-industrial residues, finding that potassium-rich biochar exhibited higher reactivity due to the catalytic role of inorganic matter. Felix et al. [14] highlighted the accuracy of TGA in monitoring mass loss and identifying optimal gasification conditions during their review of lignocellulosic and algal biomass gasification under CO_2 and steam environments. However, they emphasized the need for incorporating advanced analytical techniques for enhanced product characterization. Yousef et al. [15] employed an integrated TG-FTIR-GC-MS system to study the pyrolysis and gasification kinetics of mango seed shells under N_2 and CO_2 atmospheres. Their results demonstrated that CO_2 gasification produced a higher CO-to-H_2 ratio. Nevertheless, challenges exist in achieving consistent performance due to the variability in biomass composition and reaction conditions.

Despite promising findings, significant research gaps remain, particularly in the variability of biomass types, the lack of systematic and comprehensive exploration of suitable lignocellulosic biomass, and its ranking for CO_2 gasification. Most research has only analyzed one type of biomass, which fails to provide a comprehensive understanding of the broader applicability of CO_2 gasification processes with various biomasses. It becomes apparent that it is important for the industries to decide and select the biomass suitable for the CO_2 gasification because lignocellulosic biomass varies in structural composition and component fractions [16]. Furthermore, characterization studies or TGA analyses, if done alone, cannot offer valuable insights as they are insufficient for determining the suitability of biomass.

Therefore, the current study systematically conducted physicochemical characterizations, TGA, and kinetic analysis of five different Malaysian biomass to rank the biomass for the CO_2 gasification process. By developing a ranking framework, researchers and industries can prioritize biomass types based on their performance, paving the way for the practical implementation in CO_2 gasification. This study also incorporates catalytic investigations during TGA to further explore the influence of catalysts (dolomite and olivine) on the CO_2 gasification mechanisms. The novelty of the research encompasses: (i) the analysis of five typical lignocellulosic biomasses using thermogravimetric analysis (TGA) to assess their gasification behavior, kinetic, and thermodynamic parameters in a CO_2 environment; (ii) comprehensive physicochemical characterization of the biomasses; and (iii) the final ranking of biomass suitability for gasification based on the above criteria. Thus, by focusing on raw biomass and expanding the comparative framework, this study contributes original and impactful insights to the scientific world and industry.

2. Materials and methods

2.1. Materials

In this study, five distinct biomass types were employed, namely empty fruit bunches (EFB, *Elaeis Guineensis*), palm kernel shell (PKS, *Elaeis Guineensis*), sawdust (SD, *Neobalanocarpus Heimii*, *Hevea Brasiliensis*, *Tectona Grandis*), rice husk (RH, *Oryza Sativa*), and coconut shell (CS, *Cocos Nucifera*). These biomasses were classified based on their origin, with EFB, PKS, and RH representing agricultural and industrial milled biomass, SD as industrial manufacturing biomass, and CS as agricultural biomass. EFB and PKS were sourced from local palm oil mills, SD from a local wood furniture processing factory, RH was purchased online from the local market, and CS was obtained from a local wet market. Before conducting biomass characterization and thermogravimetric analysis (TGA) experiments, the collected biomass samples were dried in an oven at 105 °C for 24 h. Once dried, the biomass was crushed and ground using a laboratory grinder, followed by sieving through a laboratory sieve to achieve a uniform particle size of less than 250 μm, essential for ensuring homogeneity and reproducibility during experimental analysis. The catalysts used in the experiments were

dolomite (sourced from the local Malaysian market, Perlis Dolomite Industries Sdn. Bhd.) and olivine (procured from American Elements, USA). Dolomite and olivine were selected due to their natural abundance, low cost, and proven effectiveness in biomass gasification [17,18], and they are market-ready, which makes it easier for the industries to source. They were subjected to calcination (in a furnace at 800 °C for 1 h in air) to activate the catalyst for the reaction. The calcined catalysts were mixed in situ with the biomass samples for the TGA experiments.

2.2. Biomass characterization

The raw biomass was subjected to a comprehensive set of characterization analyses, including proximate, ultimate (elemental), calorific value, lignocellulosic composition, mineral content, crystallinity, and functional group.

The proximate analysis provides essential data on the moisture content (MC), volatile matter (VM), fixed carbon (FC), and ash composition of the biomass samples. Thermogravimetric analysis (TGA) is widely employed to detect proximate analysis under inert atmospheres such as nitrogen [19,20] and carbon dioxide [21], adhering to the ASTM E1131-20 standard [22]. The calorific value, which determines the higher heating value (HHV) of the biomass, was measured using an oxygen calorimeter (IKA 3000, Staufen, Germany) per the ASTM D5865 standard [23]. The HHV is determined based on Eq. (1).

$$HHV = \frac{Q}{m_{biomass}} \quad \text{Eq. 1}$$

where $m_{biomass}$ is the mass of biomass and Q is the heat released by the combustion (Joule), as shown in Eq. (2).

$$Q = C_{cal} \times \triangle T \quad \text{Eq. 2}$$

where C_{cal} is the water equivalent of a calorimeter (2883 Cal/°C) and $\triangle T$ is a rise in temperature (°C).

The ultimate analysis, which quantifies carbon, hydrogen, nitrogen, sulfur, and oxygen contents, was performed using a CHNS Analyzer (LECO CHNS-932, Mönchengladbach, Germany) in compliance with ASTM D5373-21 [24]. Lignocellulosic composition, including hemicellulose, cellulose, and lignin, was conducted using the Laboratory Analytical Procedure (LAP) developed by the National Renewable Energy Laboratory (NREL), USA [25].

The chemical and structural compositions of the biomass, particularly its functional groups, were then analyzed using Fourier Transform Infrared (FTIR) spectroscopy (Thermo Scientific, Nicolet iS20, Waltham, Massachusetts, USA) to prove the existence of cellulose, hemicellulose, and lignin in biomass. The IR spectra of the samples were recorded at room temperature over a wavelength range of 4000 to 400 cm^{-1}.

Mineral analysis was done using an X-Ray Fluorescence (XRF) Analyzer (Rigaku Primus IV, Tokyo, Japan), adhering to the ASTM E572 standard [26]. The crystallinity of the biomass, particularly its cellulose fraction, was determined using X-ray Powder Diffraction (XRD) analysis (Bruker D8 Discover, Billerica, Massachusetts, USA) [27]. Crystallinity plays a critical role in determining the reactivity and accessibility of biomass during thermal and chemical processes. Natural cellulose comprises glucose chains held together by intermolecular hydrogen bonds, forming an organized and rigid crystal structure [28]. In contrast, hemicellulose consists of disordered long chains, and lignin is an amorphous, optically inactive heteropolymer [29]. XRD analysis classifies hemicellulose and lignin as amorphous components, while the crystallinity of cellulose depends on its structural organization. Other factors, such as wax concentration and fatty acid composition, may also influence the overall crystallinity of biomass [30]. High-crystallinity zones exhibit strong resistance to chemical alteration, making them difficult to penetrate, while amorphous regions are more accessible and reactive to chemical and thermal processes. Consequently, lower crystallinity is advantageous for biomass gasification, as it facilitates higher reactivity and process efficiency.

The crystallinity index of cellulose I in the biomass was calculated using the Segal equation [31], which is expressed in Eq. (3).

$$CrI = \frac{I_{200} - I_{am}}{I_{200}} \times 100 \quad \text{Eq. 3}$$

Where, CrI is Segal crystallinity index, I_{200} is the crystalline peak and I_{am} is the amorphous peak intensity value. Specifically, this refers to cellulose I, the naturally occurring crystalline form of cellulose. Cellulose can exist in different polymorphic forms, including cellulose II, III, and IV, which arise through various chemical or thermal treatments. However, in most native biomass, cellulose I is the predominant form [29].

2.3. Biomass-CO_2 gasification using thermogravimetric analyzer (TGA) with and without catalyst

Thermal decomposition of biomass, both individually and in the presence of catalysts (5 wt% olivine or 5 wt% dolomite), was investigated using a thermogravimetric analyzer (Mettler Toledo TGA, 3+ Star System, Ohio, USA). In the TGA experiments, the biomass samples were crushed, ground, and sieved to a uniform particle size of less than 250 μm [32]. This small particle size increased the surface area and enhanced heat transfer efficiency, thereby minimizing both internal and external heat and mass transfer limitations [33].

Approximately 10 mg of biomass sample was loaded into the TGA machine for each experiment. The temperature was systematically increased from room temperature to 900 °C, at heating rates of 5, 10, and 20 °C/min. CO_2 gas was continuously purged into the TGA chamber at a 50 mL/min flow rate throughout the process. To ensure uniformity in the catalytic cases, the biomass and catalyst were thoroughly mixed by a vigorous shaker in a sample tube before loading into the TGA to ensure well-mixed conditions.

2.4. Kinetic analysis

Thermogravimetric data were used to determine the kinetic parameters of the reactions involved in the thermal degradation of biomass. The fundamental equation governing the rate of conversion (α) is given by Eq. (4) and Eq. (5):

$$\alpha = \frac{m_i - m_T}{m_i - m_f} \quad \text{Eq. 4}$$

$$\frac{d\alpha}{dt} = f(\alpha)\, k(T) \quad \text{Eq. 5}$$

where α is the degree of conversion (fractional mass loss); m_i, m_T, and m_f represents the initial mass, the mass at temperature T, and the final mass of the sample, respectively; $f(\alpha)$ is the reaction model function, described by Eq. (6) for n^{th}-order kinetics; and $k(T)$ is the temperature-dependent rate constant, expressed by the Arrhenius equation (Eq. (7)).

$$f(\alpha) = (1 - \alpha)^n \quad \text{Eq. 6}$$

$$k(T) = Ae^{\left(-\frac{E_a}{RT}\right)} \quad \text{Eq. 7}$$

where A is the pre-exponential factor (min^{-1}), E_a is the activation energy (kJ/mol), R is the ideal gas constant (J/mol.K), T is the temperature (K).

Kinetic parameters, such as activation energy (E_a), can be determined by analyzing the temperature-dependent mass loss behavior of biomass (TG/DTG data) at varying heating rates. This method, known as iso-conversional kinetic analysis, is widely utilized for estimating the E_a of complex reactions, including the thermal decomposition of biomass under constant heating rate (β, °C/min), Eq. (8) [34].

$$\beta = \frac{dT}{dt} \quad \text{Eq. 8}$$

where T is temperature (°C) and t is time (min).

Eq. (5) is modified by considering β to form the basis for the kinetic analysis, as shown in Eq. (9).

$$\frac{d\alpha}{dt} = \frac{f(\alpha)k(T)}{\beta} \quad \text{Eq. 9}$$

Substituting Eq. (6) and Eq. (7) into Eq. (9) yields the differential form of the reaction rate, as defined by Eq. (10).

$$\frac{d\alpha}{dt} = \frac{A}{\beta} e^{\left(\frac{-E_a}{RT}\right)} (1-\alpha)^n \quad \text{Eq. 10}$$

Eq. (11) shows the integrated form of the reaction rate, $g(\alpha)$. Since the degradation rate of biomass is negligible at ambient temperature, the lower limit can be excluded, as shown in Eq. (12).

$$g(\alpha) = \int_0^{\alpha} \frac{d\alpha}{f(\alpha)} = \frac{A}{\beta} \int_{T_0}^{T} e^{\left(\frac{-E_a}{RT}\right)} dT \quad \text{Eq. 11}$$

$$g(\alpha) = \frac{A}{\beta} \int_0^{T} e^{\left(\frac{-E_a}{RT}\right)} dT = \frac{AE_a}{\beta R} p(u) \quad \text{Eq. 12}$$

Here, $u = \frac{E_a}{RT}$ represents the temperature-dependent exponential integral, which lacks an analytical solution. Nevertheless, various approximations have been developed to solve Eq. (12) using iso-conversional methods. In this study, three such model-free methods were employed, including the Flynn-Wall-Ozawa (FWO), Starink (STK), and Kissinger-Akahira-Sunose (KAS) methods. They are commonly employed for their widespread application, reliability, rational assumptions, and compatibility with thermogravimetric analysis (TGA) data [12,35]. Each method applies a distinct approximation to solve for the apparent activation energy (E_α) and the pre-exponential factor (A).

For the FWO method, substituting the temperature integral approximation $p(u) = -5.331 - 1.0516u$ into Eq. (12) yields the first-order non-isothermal kinetic rate expression presented in Eq. (13) [36]. From this equation, E_α and A can be determined from the slope and intercept of the plot of ln (β) against $\frac{1}{T_m}$.

$$FWO: \ln(\beta) = \ln\left(\frac{AE_a}{R.g(\alpha)}\right) - 5.331 - 1.0516\frac{E_a}{RT_m} \quad \text{Eq. 13}$$

In the STK method, the approximation $p(u) = \frac{e^{-1.0008u} - 0.312}{u^{1.92}}$ is used in Eq. (12), resulting in the rate law given in Eq. (14) [36]. Here, E_α and A are also derived from the slope and intercept of the linear plot between $\ln\left(\frac{\beta}{T_m^{1.92}}\right)$ and $\frac{1}{T_m}$.

$$STK: \ln\left(\frac{\beta}{T_m^{1.92}}\right) = \ln\left(\frac{AR^{0.92}}{E_a^{0.92} g(\alpha)}\right) - 0.312 - 1.008\frac{E_a}{RT_m} \quad \text{Eq. 14}$$

Similarly, the KAS method employs the approximation $p(u) = u^{-2}e^{-u}$ into Eq. (12), leading to the rate expression in Eq. (15) [36]. From Eq. (15), the E_α and A are obtained from the slope and intercept of the corresponding plot between $\ln\left(\frac{\beta}{T_m^2}\right)$ and $\frac{1}{T_m}$.

$$KAS: \ln\left(\frac{\beta}{T_m^2}\right) = \ln\left(\frac{AR}{g(\alpha).E_a}\right) - \frac{E_a}{RT_m} \quad \text{Eq. 15}$$

where β is the heating rate; A is pre-exponential factor; E_a is activation energy; R is ideal gas constant; $g(\alpha)$ is a constant at a given value of conversion; T_m is the temperature of the maximum peak observed in the DTG curve.

2.5. Thermodynamic analysis

Thermodynamic analysis helps elucidate the energetic and molecular behavior of biomass thermal decomposition by evaluating enthalpy (ΔH), Gibbs free energy (ΔG), and entropy (ΔS) changes [34]. These thermodynamic parameters are calculated using the relationships outlined in Eq. 16-Eq. (18).

$$\Delta H = E_a - RT \quad \text{Eq. 16}$$

$$\Delta G = E_a + RT_m \ln\left(\frac{k_B T_m}{hA}\right) \quad \text{Eq. 17}$$

$$\Delta S = \frac{\Delta H - \Delta G}{T_m} \quad \text{Eq. 18}$$

where, k_B is the Boltzmann constant (1.381×10^{-23} J K^{-1}), T_m is the temperature of the maximum peak observed in the DTG curve, h is the Planck constant (6.626×10^{-34} J/s), and A is the pre-exponential factor $\left(\beta.E_a.e^{(-E_a/RT_m)}/RT_m^2\right)$.

The parameter ΔH provides insight into the thermal nature of the reaction, indicating whether the process is endothermic (requiring heat input) or exothermic (releasing heat). This characterization helps to understand the heat dynamics of the reaction. ΔG evaluates the spontaneity of the reaction, particularly the formation of the activated complex. The sign and magnitude of ΔG are crucial, with a negative ΔG signifying a spontaneous process and a positive ΔG indicating reduced spontaneity [37]. ΔS quantifies the degree of disorder or randomness in the system. This parameter provides additional context for the molecular changes occurring during the reaction, complementing the enthalpy and Gibbs free energy data.

2.6. Biomass ranking methodology

The feasibility of biomass utilization was systematically evaluated through a two-tiered analytical approach. In the first tier, the physical characterization of biomass was conducted, emphasizing key performance indicators such as fixed carbon (FC), ash content (ASH), elemental composition (C and H), cellulose, lignin, potassium (K), calcium (Ca), iron (Fe), and the crystallinity index (CrI). These indicators were assessed for suitability of the gasification process, with higher values generally preferred for most parameters except ASH and CrI, where lower values indicated better performance. Each biomass type (EFB, PKS, SD, RH, and CS) was scored individually for each performance metric. The cumulative scores were then used to rank the biomass types based on their feasibility for gasification applications.

The second tier focused on thermogravimetric analysis (TGA) experiments using CO_2 as the reacting agent, both with and without the inclusion of catalysts. Dolomite (DOL) and olivine (OLI) were employed as catalysts to assess their impact on gasification performance. Two critical indicators were analyzed: activation energy (Ea) during Stage II decomposition and the Gibbs free energy change (ΔG). Lower values for both indicators were deemed favorable, reflecting enhanced reactivity and thermodynamic feasibility. Combined scores from these experiments were computed to evaluate and rank biomass-catalyst combinations. The overall research workflow for this study is provided in Fig. 1.

3. Results and discussion

3.1. Proximate and ultimate analysis and calorific value

Proximate, ultimate, and calorific values of five biomasses are shown in Table 1, and the values are compared with the literature. The variation between the present study and literature values could be due to the

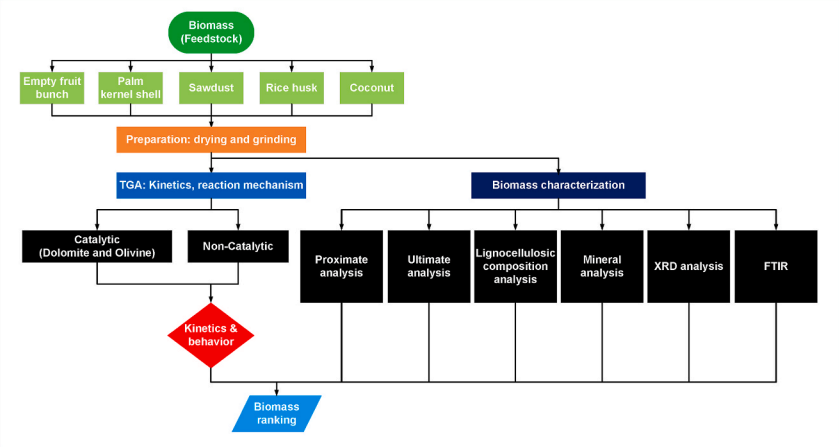

Fig. 1. Schematic overview of the research workflow.

Table 1
Comparison of the proximate, ultimate, and HHV values of five different biomass samples.

Proximate analysis						
Biomass	Moisture content (wt.%)	Volatile matter (wt.%)	Fixed carbon (wt.%)	Ash (wt.%)	HHV (MJ/kg)	References
EFB	6.51	74.92	14.44	4.14	16.52	This study
	7.50	75.00	10.50	7.00	15.61	[42]
PKS	9.48	80.91	1.39	8.22	17.22	This study
	9.40	82.50	1.40	6.70	18.74	[43]
SD	6.84	77.13	13.02	3.01	17.10	This study
	9.20	75.46	13.80	1.54	15.09	[44]
RH	7.56	64.68	11.82	15.94	15.06	This study
	6.40	62.00	15.10	16.50	17.14	[45]
CS	6.18	72.51	19.96	1.35	18.75	This study
	5.40	67.60	22.30	4.70	15.16	[45]

Ultimate analysis						
Biomass	Carbon (wt.%)	Hydrogen (wt.%)	Nitrogen (wt.%)	Oxygen (wt.%)[a]	Sulfur (wt.%)	References
EFB	47.30	5.80	0.80	46.10	<0.05	This study
	45.50	5.90	1.20	46.50	0.70	[46]
PKS	51.10	4.70	0.40	43.80	<0.05	This study
	50.60	6.50	8.40	34.50	0.00	[46]
SD	46.10	5.30	3.60	45.00	<0.05	This study
	48.88	6.04	3.16	37.41	0.45	[47]
RH	39.50	5.00	0.50	55.00	<0.05	This study
	36.80	4.40	0.60	42.10	<0.05	[48]
CS	45.00	4.90	0.10	50.00	<0.05	This study
	48.02	6.40	0.10	44.88	0.60	[49]

[a] Oxygen is calculated by difference.

geographical conditions, planting conditions, climatic variation, and storage conditions of the biomass samples [38]. Notably, the standard deviation between experimental and literature data is less than 5 %. The moisture content in all the biomass samples was lower than 10 wt%, reducing the energy required to dry the biomass and making it suitable for the thermochemical process. The biomass predominantly comprises a high volatile matter (VM) content, ranging from 65 to 81 wt%. PKS had the highest VM content among the biomass, followed by SD, EFB, CS, and RH. The high VM in biomass indicates that high reactivity is well-suited for thermochemical energy conversion processes such as pyrolysis and gasification to generate syngas [39]. The VM will decompose into small hydrocarbons and CO under low oxygen conditions [40]. The VM parameter not only determines the quantity of syngas produced but also assesses the biomass feedstock's ignition potential and efficiency in thermal conversion [41].

When the VM of biomass is high, the fixed carbon (FC) content will be relatively low [41]. Biomass contains moderate FC, ranging from 1 to 20 wt%. CS, EFB, and SD showed high FC values (>10 wt%). The ash content was lowest for CS (1 wt%), which has the advantage of lower slagging, fouling, and erosion formation during the gasification process, while RH showed the highest (16 wt%). The calorific value usually correlates with the amount of VM and FC in the biomass, and it provides information on the energy that the biomass can supply during the gasification/pyrolysis process [50]. The calorific values of all the biomasses range between 15 MJ/kg and 17.5 MJ/kg, which is consistent with reported literature values: EFB (15.61 MJ/kg) [42], PKS (18.74 MJ/kg) [43], sawdust (SD) (15.09 MJ/kg) [44], rice husk (RH) (17.14 MJ/kg) [45], and coconut shell (CS) (15.16 MJ/kg) [45]. Overall, the ranking of the positive effects of high VM on syngas production is PKS >SD > EFB > CS > RH. In contrast, the ranking of the positive effects of low ash content is CS < SD < EFB < PKS < RH.

During CO_2 gasification, it is desirable to have a high carbon and FC content in the biomass. They are a key component of the gasification reaction, as they react with CO_2 and steam to produce syngas ($CO + H_2$). Low nitrogen and sulfur content are desirable for low NO_x and SO_x emissions. The ultimate data agree with the literature with slight deviation [47–49,51]. PKS showed the highest carbon content, whereas RH showed the least. Hydrogen contributes to the calorific value of the

syngas and reacts with oxygen or carbon to form H_2O or CH_4. Overall, the ranking of the biomasses based on high carbon content is: PKS > EFB >SD > CS > RH, whereas the ranking based on high hydrogen content is EFB >SD > RH > CS > PKS.

3.2. Lignocellulosic composition analysis

The lignocellulosic composition (cellulose, hemicellulose, and lignin) of biomass is critical in estimating the gas fraction produced during gasification. Cellulose and hemicellulose are thermally labile and decompose at relatively lower temperatures (200–400 °C), contributing to higher volatile matter release and increased gas production [52]. The rapid decomposition of these polysaccharides favors the formation of CO, H_2, and CH_4, making biomass with high cellulose and hemicellulose content more suitable for gasification and hydrogen-rich syngas production. In contrast, lignin is more thermally resistant, degrading over a broader temperature range (250–900 °C). This leads to higher fixed carbon and char formation [52]. Table 2 presents the cellulose, hemicellulose, and lignin content of various biomass types (EFB, PKS, SD, RH, and CS) obtained in this study. The values were comparable to those reported in the literature, with a minor variation of 6.5 %.

In this work, most biomass comprises cellulose and hemicellulose, except the PKS, which contains higher lignin content. The ranking of the positive effects of high cellulose content on syngas production is SD > EFB > RH > CS > PKS. In contrast, the ranking of the positive effects of high hemicellulose content on syngas production is EFB > CS > PKS > RH > SD.

3.3. FTIR analysis

The FTIR spectrum for all the biomass samples was similar and exhibited multiple bands and peaks of varying intensities, corresponding to the biomass chemical functional groups (Fig. 2). The high-energy part of the spectrum is often defined by bands or peaks spanning from 4000 to 1500 cm^{-1}. Several absorption bands frequently observed in biomass are reported by the peaks at 1102 to 1158 cm^{-1} (C-O stretching vibrations), 1317 to 1318 cm^{-1}, and 1370 to 1371 cm^{-1} (C-H bending vibrations), 1412 to 1423 cm^{-1} (C-H bending vibrations and deformation modes in carbonate or carboxylate groups), and 2898 to 2923 cm^{-1} (C-H stretching vibrations in aliphatic). These absorption patterns indicate the presence of cellulose, hemicelluloses, lignin, ethers, alcohols, carbohydrates, aliphatic hydrocarbons or methyl groups, phenolic compounds, syringyl, guaiacyl, aliphatic hydrocarbons, methoxy groups, carboxylate groups ($-COO^-$), carbonate groups (CO_3^{2-}), aromatic rings compounds, methylene groups ($-CH_2-$), methyl groups ($-CH_3$), lipids and waxes, and volatile organic compounds. Hemicellulose and lignin are dominated by ether bonds, with hemicellulose containing a substantial amount of carboxyl groups [58].

Alcohols, phenols, lignin, and other carbohydrates have free or intermolecularly linked -OH groups that emit a wide range from 3650 to 3000 cm^{-1} [59]. However, the band may also be attributed to surface-bound water symmetric and asymmetric stretching vibrations [60]. High moisture content can lower the gasification temperature; however, some moisture is necessary for steam gasification, which enhances hydrogen production. Sharp peaks from 1412 to 1423 cm^{-1} and 2898 to 2923 cm^{-1} are caused by symmetric and asymmetric C-H stretching vibrations of aliphatic -CH3- and $-CH_2-$ groups [61], indicating the presence of lignin and extractives. Furthermore, carboxylic acids, ketones, esters, and aldehydes were found to have characteristics of C=O stretching vibrations at 1370 to 1371 cm^{-1} [62]. Aliphatic and aromatic structures are key components of volatile matter in biomass. These compounds decompose into lighter hydrocarbons, CO, and H_2 during gasification, contributing to syngas formation. The presence of aromatic structures may also lead to tar formation. Carbonyl groups may decompose into CO and CO_2. Ethers, esters, and alcohol functional groups contribute to producing syngas components like CO, H_2, and CH_4. Lignin-derived aromatics can contribute to tar formation. Aliphatic and aromatic groups (part of the volatile matter) contribute to the release of hydrocarbons and the formation of char, which can further react with CO_2 or steam to produce additional syngas.

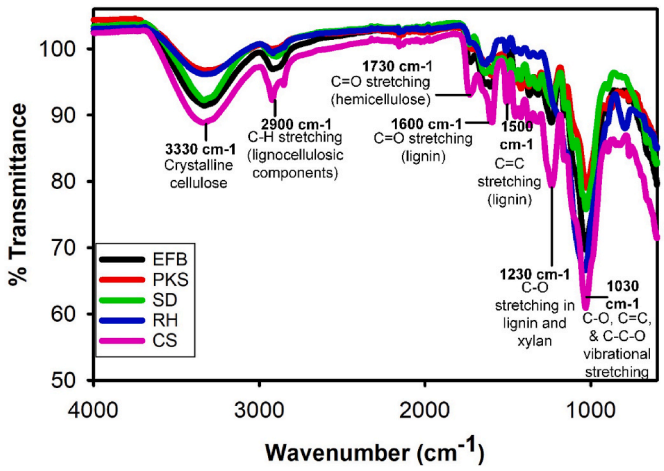

Fig. 2. FTIR spectra for EFB, PKS, SD, RH, and CS biomasses.

3.4. Mineral analysis

The major mineral oxides detected by XRF in biomass (Table 3 and Fig. 3) were Na_2O, MgO, Al_2O_3, SiO_2, P_2O_5, SO_3, Cl, K_2O, CaO, Fe_2O_3, ZnO, and TiO_2, accounting for the concentrations above 1 wt% to 89.60 wt%. The mineral oxides concentration below 1 wt% (0.00–0.72 wt%) were CuO, Br, Cr_2O_3, MnO, Rb_2O, SrO, NiO, ZrO_2, BaO, PbO, CO_2O_3, and As_2O_3.

The presence of mineral elements has a significant impact on the

Table 2
Comparison of lignocellulosic composition of five different biomass samples from this study with the literature values.

Biomass	Lignocellulosic components (wt.%)			
	Cellulose	Hemicellulose	Lignin	References
EFB	33.61	21.96	19.72	This study
	35.20	19.60	44.30	[53]
PKS	13.27	18.21	44.75	This study
	33.03	23.82	45.59	[54]
SD	36.52	10.72	32.08	This study
	42.67	16.05	23.73	[55]
RH	31.74	15.16	38.03	This study
	32.65	18.08	26.68	[56]
CS	22.30	20.21	36.18	This study
	33.61	29.27	36.51	[57]

Table 3
Primary mineral oxides content of five biomass samples.

Mineral	Mineral content of biomass (wt. % dry ash)				
	EFB	PKS	SD	RH	CS
Na_2O	0.00	0.13	0.07	0.01	1.24
K_2O	49.10	2.35	3.45	3.34	57.30
MgO	1.95	1.09	0.71	0.40	2.23
CaO	10.70	24.10	20.50	1.30	9.66
Al_2O_3	1.13	7.93	1.84	0.28	0.06
Fe_2O_3	7.48	41.60	3.48	1.23	3.34
ZnO	0.54	0.04	0.24	0.05	0.21
TiO_2	0.40	0.45	62.30	0.00	0.00
SiO_2	16.10	19.30	3.50	89.60	6.33
P_2O_5	2.17	1.18	0.61	0.86	3.17
SO_3	3.95	1.13	1.25	1.70	4.67
Cl	5.18	0.35	1.12	0.71	11.20

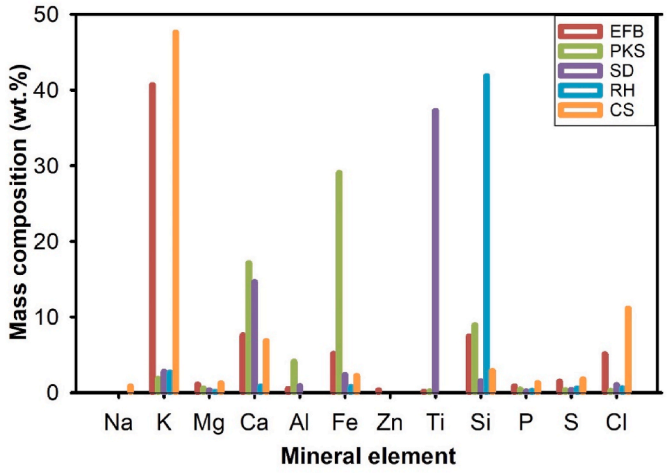

Fig. 3. Primary mineral composition of EFB, PKS, SD, RH, and CS biomasses.

gasification process. Nonetheless, the mineral elements with the highest catalytic effect on gasification are unknown [46]. Alkali and alkaline earth metals (AAEMs) may influence the viability of biomass feedstock in recovering energy or producing syngas. Numerous studies have proved that high AAEM content in the feedstock improves gasification performance due to the catalytic effects of metal minerals present in biomass [63,64]. Metal oxide catalysts reduce the starting temperature and enhance reaction rates regardless of the gasification medium, but only up to a certain point. According to Refs. [65,66], K has greater catalytic activity on CO_2 gasification rates than other alkali minerals. The introduction of metal catalysts in the sequence K > Na > Ca > Fe > Mg increased the CO_2 gasification reactivity of the feedstock. Hence, RH may show the lowest CO_2 gasification reactivity as it mainly consists of non-AAEMs. In contrast, other biomasses may show high gasification reactivity due to their high AAEM content, particularly the CS and EFB.

CS and EFB mainly contain potassium (K), with dry ash mass percentages of 47.60 wt% and 40.70 wt%, respectively (Fig. 3). The values agree with Ahmad et al. [67] and Novianti et al. [68], who reported that K_2O is the main mineral in CS and EFB. PKS mainly contains iron (Fe), with 41.60 wt% of Fe_2CO_3, which contradicts the literature data reported by Sohni et al. [69], Hussain et al. [70], and Ikubanni et al. [71], in which their PKS consists of 1–3 wt% of Fe_2O_3. This may be due to the grinding process, during which some tiny Fe particles from the grinder bales might have mixed with the biomass. Besides Fe, Ca is another significant mineral in PKS, which is consistent with the results of Sohni et al. [69]. Surprisingly, SD contains a large amount of titanium (Ti) (37.30 wt%), which also contradicts previous studies [72,73]. They found calcium (Ca), K, silica (Si), and negligible quantities of Ti. It may be due to the painting material of the wood or the sawing process that has contributed to the Ti content in the SD sample. Although Ti composition differs from previous studies, other major minerals (i.e., Ca, K, and Si) are consistent with the literature data. RH contains Si (41.90 wt%), consistent with other reported literature [69].

However, some studies have shown that biomass with a high AAEM content is susceptible to contamination, sintering, and agglomeration during larger-scale gasification, particularly in fluidized bed reactors [74,75]. The mineral component in the biomass varies according to the type of biomass. Biomasses with extremely high ash and mineral content are prone to pre-treatment (washing, acid treatment) before gasification to avoid contamination, sintering, and agglomeration.

Higher metal content, especially alkali and alkaline earth metals such as calcium (Ca) and potassium (K), usually improves the catalytic effect during gasification. The ranking of the positive impact of high Ca content is PKS >SD > EFB > CS > RH, whereas the hierarchy of the positive effects of high K content is CS > EFB >SD > RH > PKS. The ranking of the positive impact of high Fe content is PKS > EFB >SD > CS > RH.

3.5. Crystallinity analysis

The XRD profiles (Fig. 4) show the existence of well-defined crystalline peaks in various biomasses corresponding to cellulose at 2θ ranges from 8.39° to 16.06° and 20.54°–22.5°, proving the existence of cellulose in all biomasses. The Segal crystallinity index (CrI) was observed in increasing order: PKS (17.8 %), EFB (20.7 %), CS (25.1 %), SD (35.0 %), and RH (37.3 %). High CrI may reduce the depolymerization rates, leading to a lower gasification rate [76]. A lower CrI indicates a higher proportion of amorphous cellulose, which enhances the biomass's reactivity during gasification [77]. Hideno [78] has demonstrated that reducing cellulose crystallinity decreases its thermal degradation temperature, accelerating the decomposition process. In this work, the positive effect ranking of low crystallinity on syngas production is PKS < EFB < CS < SD < RH.

3.6. TG-DTG profiles of biomass gasification under CO_2 environment

Fig. 5 depicts the TG and DTG profiles of biomass samples with and without catalysts in the CO_2 environment. The moisture loss took place between 30 °C and 150 °C. The weight loss between 275 °C and 300 °C corresponds to the decomposition of hemicellulose, whereas the weight loss between 350 °C and 400 °C corresponds to the decomposition of cellulose. Lignin typically degrades across an extensive temperature range, from 280 °C to 450 °C.

Above 500 °C, the CO_2 gasification of fixed carbon lasts over a wide temperature range, from 380 °C to 900 °C. CO_2 gas was relatively inert within the initial temperature range from room to 700 °C. Higher temperatures are required to promote the reaction between the fixed carbon (obtained from biomass) and CO_2, since the Boudouard reaction between carbon and CO_2 ($C + CO_2 \rightleftarrows 2CO$) occurs at temperatures above 700 °C [79]. CO_2 significantly improved the gasification process of most biomass samples, particularly those with a high fixed carbon content, by increasing the yield of syngas because of the reaction between fixed carbon and CO_2 [79]. At temperatures above 700 °C, EFB with catalysts showed an additional peak on the DTG curves, indicating significant weight loss, leaving minor residues after gasification. Other biomasses (PKS, SD, and CS) with catalysts also showed an additional DTG peak above 700 °C, which indicates the Boudouard reaction due to the higher energy available at this temperature. The difference in the degradation pattern during catalytic gasification might be attributed to the catalytic activity or heat and mass transfer limits.

In summary, the interaction between the CO_2 and biomass in the temperatures (room temperature to 700 °C) is very limited or negligible, with a TG/DTG profile almost similar to pyrolysis or in an inert atmosphere. Syngas production is expected to be low at this stage (room temperature to 700 °C), with a high amount of tar production (condensable volatile matter), undesirable for gasification. The energy above 700 °C is enough to initiate the Boudouard reaction (carbon + CO_2) that can produce CO and other gaseous products. The TGA data signifies that the temperature in a large-scale gasification plant should be higher than 700 °C to maximize syngas production. The catalyst (dolomite and olivine) did not contribute significantly to the pyrolysis stage (volatilization) between room temperature and 400 °C. However, the catalytic activity increased beyond 400 °C. The effect of the catalyst was more pronounced in certain biomasses than in others. For example, the reaction between CO_2, biomass, and catalyst was evident in EFB biomass, followed by PKS, SD, CS, and RH.

3.7. Kinetic analysis of biomass gasification under a CO_2 environment

The activation energy (E_a) values, either average or depending on the extent of the gasification reaction, are essential in determining the

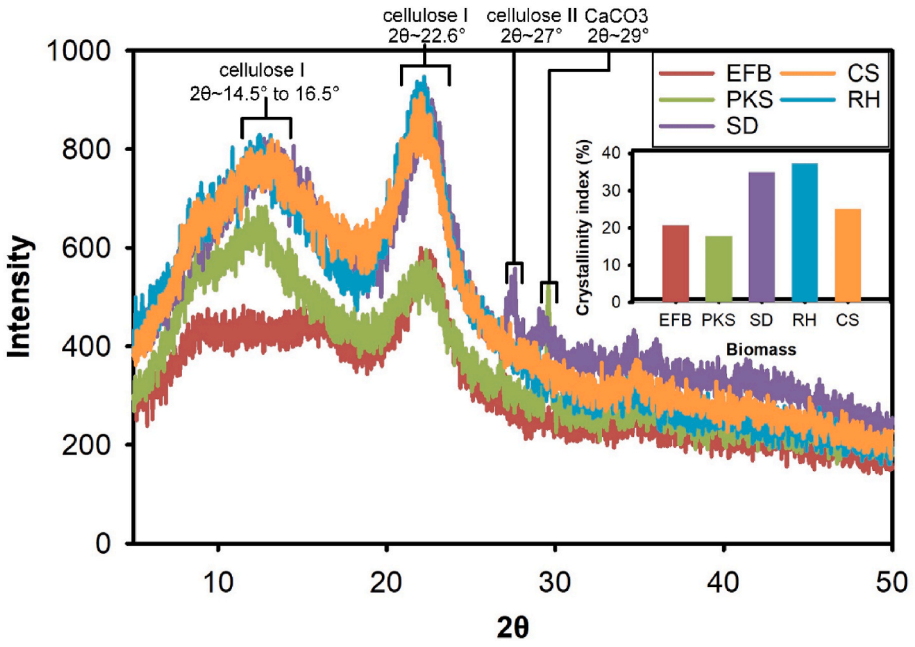

Fig. 4. XRD profiles and crystalline index of EFB, PKS, SD, RH, and CS biomasses.

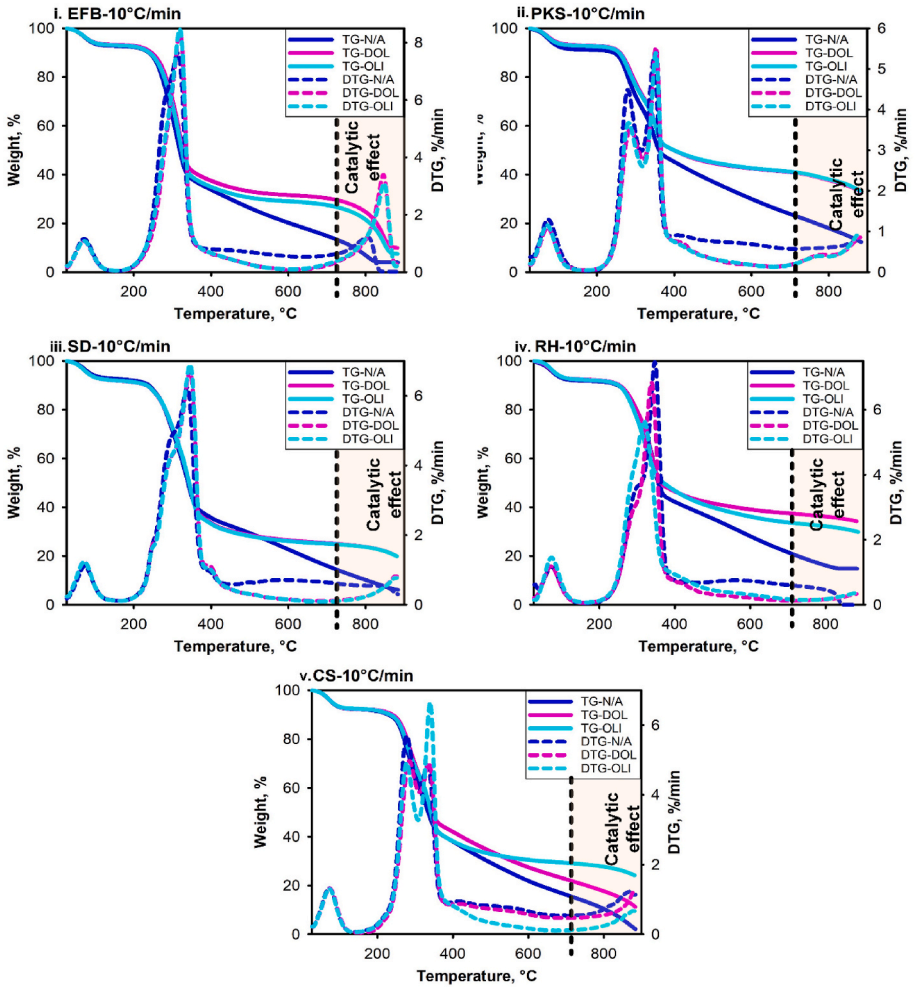

Fig. 5. TG-DTG biomass gasification profiles of five biomasses: EFB (i), PKS (ii), SD (iii), RH (iv), and CS (v) with (Dolomite (DOL) and Olivine (OLI)) and without (N/A) catalyst under CO_2 at a 10 °C/min heating rate.

feasibility of the process energy (i.e., whether the process can provide energy on its own through exothermic reaction or require external energy input). The trends of E_a against the conversion (α) (Fig. 6) for the FWO, STK, and KAS methods are almost similar, with a minor deviation. The subsequent analysis of E_a and other thermodynamic parameters is based on the averaged values derived from the three methods, offering a more generalized and robust representation of the thermal decomposition behavior. Initially, the E_a increased at 10 % conversion (attributed to the energy required to remove the moisture). From 15 % to 60 % conversion (during the pyrolysis reactions), it remained stable for EFB, SD, RH, and CS biomasses, indicating a single reaction mechanism. The E_a profile for PKS biomass differed from all other biomasses. It varied along the conversion, indicating multiple reaction mechanisms or complex kinetics, which could be due to impurities. A drop in E_a value at 60 % conversion, representing the end of biomass decomposition and char formation. Except for RH, there was a sharp increase in E_a value at 60 %, possibly due to the energy required to break the silica bonding in the biomass. The char requires minimal gasification energy, as shown by a slight or no increase in the E_a. The peak at 60 % (or high E_a) may correspond to more resistant components (e.g., lignin decomposition). The peak also indicates the transition points between different reaction stages. Lower E_a indicates the exothermic (release of energy) during the reaction, which is advantageous to the CO_2 gasification process, as less energy will be required at the higher temperature (Stage II). Biomasses such as EFB and CS with lower overall E_a is easier to gasify.

Fig. 7(i)–(ii), and (iii) depict the progression of conversion (α) with temperature for non-catalytic, dolomite-catalysis (DOL), and olivine-catalysis (OLI), respectively. Typically, all biomasses showed a low conversion rate in Stage I (devolatilization, below 380 °C) due to the inert behavior of CO_2 at low temperatures. After 380 °C (Stage II), the conversion rate accelerated due to the gasification of fixed carbon from the char with the CO_2. Catalysts (dolomite and olivine) enhanced the conversion rates compared to non-catalytic systems, especially during Stage II (Fig. 7 (iv), (v), and (vi)). E_a profiles demonstrate significant reduction and smoother trends in the presence of a catalyst (Fig. 7 (v) and (vi)), particularly for RH with dolomite, indicating improved reaction kinetics. This effect is because of a change in the reaction pathway.

In this work, negative E_a were observed for Stage II (fixed carbon gasification) under conditions involving complex, multi-step mechanisms, consistent with reports by Nasfi et al. [80] and Prajapati et al. [81]. In certain systems, an overall negative E_a can arise when a strongly exothermic surface reaction or a reverse reaction becomes dominant at higher temperatures, leading to a decline in the overall reaction rate with increasing temperature [82]. In the present case, the dominant reaction in CO_2 gasification (Boudouard reaction) is reversible. Hence, the negative apparent E_a may be attributed to this reverse reaction.

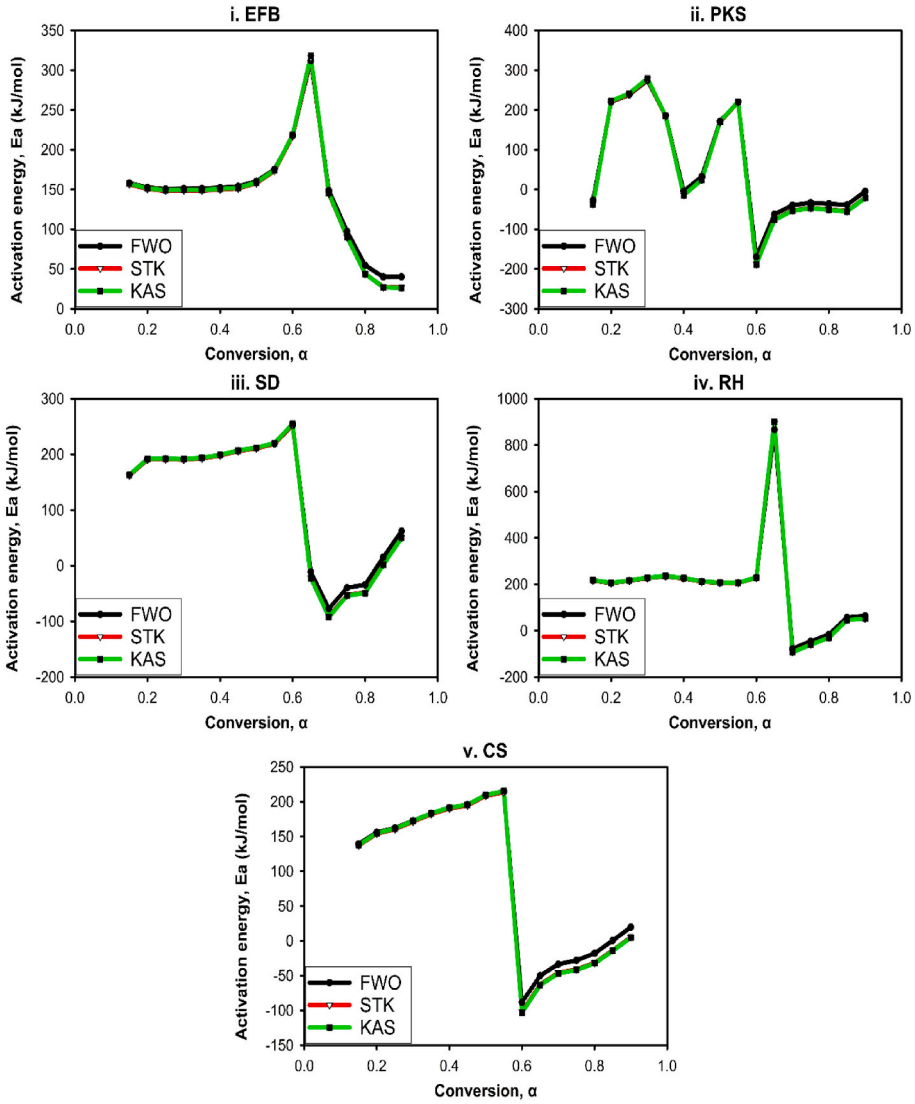

Fig. 6. Activation energy (Ea) against conversion (α) for different biomass materials (EFB, PKS, SD, RH, CS) using FWO, STK, and KAS methods.

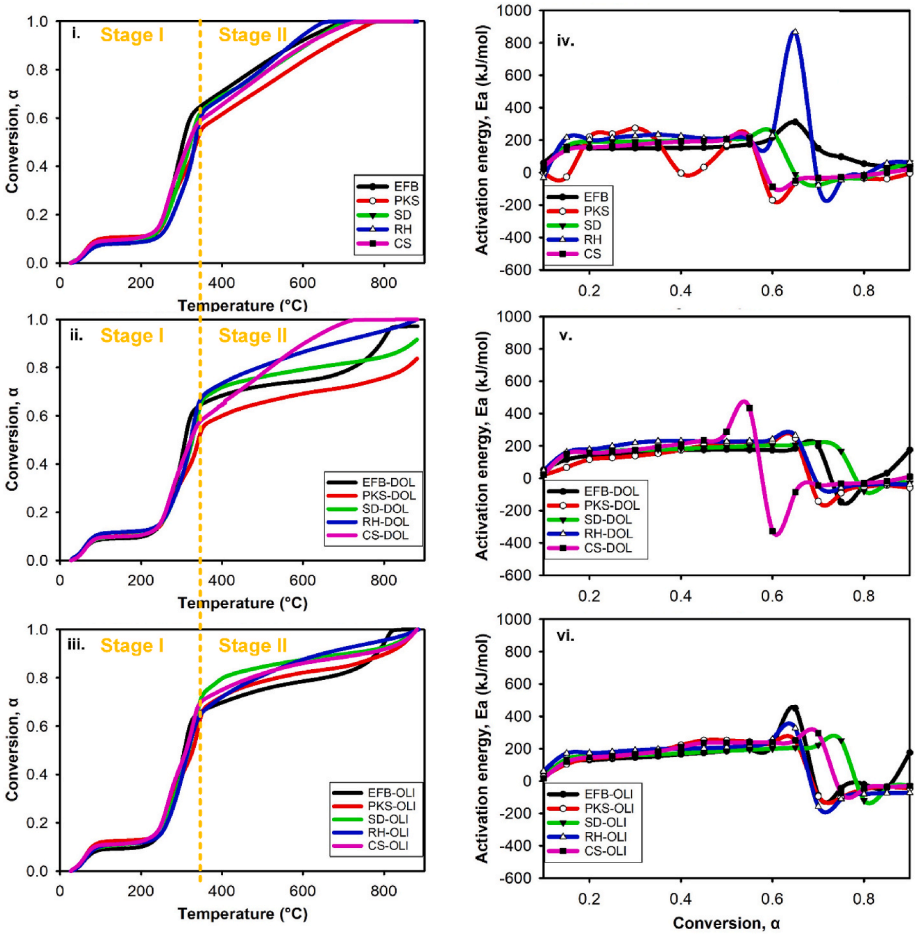

Fig. 7. Conversion profiles (10 °C/min) (i to iii), and Activation energy (Ea) (iv to vi) trends during non-catalytic and catalytic (DOL: dolomite and OLI: olivine) CO_2 gasification of various biomass types.

Additionally, other factors such as changes in char structure, or the dominance of internal diffusion and mass transfer limitations could contribute to this anomaly [82]. These effects may be amplified in thermogravimetric analyses under non-isothermal conditions, where apparent kinetic parameters can be influenced by physical rather than purely chemical phenomena. In Stage II, PKS showed the lowest E_a, followed by CS, SD, EFB, and RH. Lower E_a is ideal since it consumes less energy to initiate the reaction, particularly the Boudouard reaction. Addition of 5 wt% catalysts (dolomite and olivine) during CO_2 gasification helped further reduction in E_a at Stage II, and significant changes were observed at the higher conversions (above 0.6). This proves the active role of catalysts at higher temperatures, which might enhance syngas production. The catalysts were ineffective during Stage I of the CO_2 biomass gasification.

In summary, the catalyst played a significant role in Stage II of biomass gasification, i.e., at higher conversion above 0.6 and higher temperatures. Adding a catalyst can enhance the gas yield by changing the reaction kinetics. The ranking of the positive effects of low E_a content at Stage II will be PKS < CS < SD < EFB < RH.

3.8. Thermodynamic analysis of biomass gasification under CO_2 environment

Table 4 provides thermodynamic properties such as enthalpy change (ΔH), Gibbs free energy change (ΔG), and entropy change (ΔS) of biomass subjected to gasification reaction under CO_2 with and without a

Table 4
Thermodynamic parameters of biomass gasification in the CO_2 environment compared to those in the other gasifying environment.

Biomass	Gasifying agent	ΔH (kJ/mol)			ΔG (kJ/mol)			ΔS (kJ/K.mol)			References
		Without catalyst	+ DOL	+ OLI	Without catalyst	+ DOL	+ OLI	Without catalyst	+ DOL	+ OLI	
EFB	CO_2	131.84	112.88	115.52	150.33	150.93	150.41	−0.03	−0.01	0.04	This study
	Air	141.79	–	–	441.62	–	–	−0.30	–	–	[86]
PKS	CO_2	43.95	80.43	103.12	159.77	160.74	159.71	0.03	−0.01	0.03	This study
	Air	132.02	–	–	159.1	–	–	−0.04	–	–	[87]
SD	CO_2	105.64	126.87	122.79	158.33	158.16	158.23	−0.01	0.02	0.01	This study
	Air	155.91	–	–	185.98	–	–	−0.05	–	–	[88]
RH	CO_2	168.86	124.32	103.37	157.39	155.02	149.75	0.13	0.07	0.08	This study
	Air	214.60	–	–	178.88	–	–	0.06	–	–	[89]
CS	CO_2	76.38	79.04	128.65	141.48	146.11	156.12	0.01	0.08	0.05	This study
	Air	87.65	–	–	251.14	–	–	−0.20	–	–	[90]

+DOL: Biomass with 5 wt% dolomite; +OLI: Biomass with 5 wt% olivine.

catalyst, and the values are compared with those of air gasification from the literature. The thermodynamic properties were determined based on the average activation energy values derived from the FWO, STK, and KAS methods since the E_a values were broadly consistent among the three isoconversional methods.

The positive ΔH values (43.95–168.86 kJ/mol) show the endothermic nature of CO_2 gasification, indicating the requirement for external energy input to break reactant bonds during the decomposition stage. Lower ΔH values are favored in the gasification process as they promote the formation of the activated complex (it is a state where bonds are partially broken and new bonds are formed), thereby reducing the overall energy demand required for the reaction [37,83]. Interestingly, the average ΔH under the CO_2 environment is lower than those observed for air-based gasification because of the complexity of biomass and the heterogeneous reactions occurring during CO_2 gasification, which reduce the overall energy demand [84,85].

Positive ΔG values indicate non-spontaneous gasification processes, where external energy input is required to drive the reaction forward [37]. The ΔG values for the studied biomasses (EFB, PKS, SD, RH, and CS) are all positive, ranging from 141.48 to 159.77 kJ/mol, highlighting CO_2 gasification process does not occur spontaneously [91]. Among these biomasses, PKS, SD, and RH exhibit relatively higher positive ΔG values (159.77, 158.33, and 157.39 kJ/mol, respectively), whereas CS and EFB show relatively lower values (141.48 and 150.33 kJ/mol, respectively). This suggests that CO_2 gasification of CS and EFB requires less external energy input, making them more favorable for gasification based on their ΔG values.

The ΔS values fluctuated between positive and negative, within the −0.03 to 0.03 kJ/K.mol range, reflecting slight differences in the degree of disorder during gasification. The low positive ΔS values under CO_2 gasification conditions indicate limited reactivity, making it more challenging to form the activated complex [37]. It suggests a biomass thermochemical process shifting closer to thermodynamic equilibrium. In contrast, the negative ΔS values (such as in EFB and SD) indicate that the bond-breaking-induced disorder of gasification products is lower than that of the reactants [92]. Since ΔS values are close enough among all biomasses in this study, it is not considered in the ranking criteria.

CO_2-based gasification offers advantages over air-based gasification. Lower ΔH values indicate reduced energy requirements, and lower ΔS values suggest more controlled reactions [93]. The relatively lower positive ΔG values in CO_2 gasification underscore its thermodynamic favorability [93]. For instance, the ΔH values for CO_2 gasification, ranging from 43.95 kJ/mol to 168.86 kJ/mol, are significantly lower than those of air gasification (87.65 kJ/mol to 214.60 kJ/mol). Additionally, the ΔG for EFB-CO_2 (150.33 kJ/mol) is substantially lower than that under air gasification (441.62 kJ/mol).

Dolomite and olivine catalysts lowered the energy barrier, enhancing reaction kinetics and thermodynamic favorability [94]. For instance, ΔH for RH-CO_2 decreases from 168.86 kJ/mol (uncatalyzed) to 124.32 kJ/mol with dolomite and 103.37 kJ/mol with olivine. A similar trend is observed for EFB-CO_2, where dolomite reduces ΔH from 131.84 kJ/mol to 112.88 kJ/mol, and olivine further lowers it to 115.52 kJ/mol. These reductions demonstrate the ability of catalysts to facilitate bond-breaking and activated complex formation.

The catalytic impact of dolomite and olivine also depends on the biomass type, reflecting the inherent heterogeneity of biomass composition. In this study, PKS-CO_2, SD-CO_2, and CS-CO_2 (43.95, 105.64, and 76.38, respectively) exhibit increased ΔH with dolomite (80.43, 126.87, and 79.04 kJ/mol, respectively) and olivine (103.12, 122.79, and 128.65 kJ/mol, respectively). This increase is likely due to the specific chemical composition of each biomass type, particularly the varying proportions of lignin, cellulose, and hemicellulose, which interact distinctively with the catalysts. Such interactions influence the energy requirements of bond-breaking and reaction pathways, resulting in distinct thermodynamic values. These findings align with those reported by Wang et al. [95], emphasizing the critical role of biomass heterogeneity in determining catalytic effects and thermodynamic performance during gasification.

Catalysts primarily influence reaction kinetics rather than ΔG, which remained relatively stable [96]. In this study, the change in ΔG for EFB-CO_2 was minimal with dolomite (150.93 kJ/mol) and olivine (150.41 kJ/mol), which suggests that dolomite and olivine enhance reaction rates without significantly altering thermodynamic spontaneity [94]. Dolomite, composed of calcium and magnesium carbonates [97], aids decarbonization, while olivine, rich in magnesium silicate, enhances heat transfer and tar cracking [98].

In summary, dolomite and olivine catalysts enhance the energy efficiency of CO_2-based gasification by reducing ΔH and improving reaction kinetics, particularly for EFB and RH. Reactivity trends based on thermodynamic parameters (ΔH and ΔG) revealed the ranking of the five studied biomasses for gasification. In the CO_2 environment, CS exhibited the lowest ΔG values (141.48–156.12 kJ/mol), indicating the highest reaction spontaneity, followed by EFB, RH, SD, and PKS. Conversely, PKS demonstrated the lowest ΔH values (43.95–103.12 kJ/mol), signifying the least energy requirement for gasification, followed by CS, SD, EFB, and RH.

3.9. Biomass ranking

A comprehensive ranking of selected biomass feedstocks for CO_2 gasification is presented in Table 5 based on characteristics and thermodynamic properties. EFB emerged as the most favorable biomass among the feedstocks, achieving the highest score (45) considering the characteristics, including a balanced composition of cellulose and hemicellulose combined with low ash content and higher volatile matter, which is highly suitable for gasification.

The score is relatively close for some biomasses (PKS, CS, and SD), indicating that these feedstocks also have the potential for gasification. RH scores the least, which would be less favored for gasification due to its high silica content. It negatively affects gasification by causing slagging and fouling issues in reactors [69]. Therefore, more pre-treatment methods would be required to reduce the silicon content in RH. Further studies in lab-scale systems would demonstrate their feasibility for the gasification process.

Table 6 tabulates the biomass ranking based on thermodynamic properties with catalysts (dolomite and olivine) and compares it with those without catalysts. Notably, CS with dolomite (CS + DOL) achieved the highest ranking, followed by CS without a catalyst (CS + N/A) and RH with dolomite (RH + DOL).

The data revealed varying catalyst effectiveness across different

Table 5
Biomass ranking based on characterization and thermodynamic data.

Performance indicator	EFB	PKS	SD	RH	CS
Biomass Characterization					
↑ VM	3	5	4	1	2
↓ ASH	3	2	4	1	5
↑ C	4	5	3	1	2
↑ H	5	1	4	3	2
↑ Cellulose	4	1	5	3	2
↑ Hemicellulose	5	3	1	2	4
↑ K	4	1	3	2	5
↑ Ca	3	5	4	1	2
↑ Fe	4	5	3	1	2
↓ CrI	4	5	2	1	3
Total marks	**39**	**33**	**33**	**16**	**29**
Ranking	**1**st	**2**nd	**3**rd	**5**th	**4**th
After adding thermodynamic properties					
↓ ΔH	2	5	3	1	4
↓ ΔG	4	1	2	3	5
Total marks	**45**	**39**	**38**	**20**	**38**
Ranking	**1**st	**2**nd	**4**th	**5th**	**3**rd

↑ (high in value) and ↓ (low in value): favorable for gasification.
5 is the most favorable, and 1 is the least favorable.

Table 6
Performance ranking of biomass feedstocks with and without catalysts for thermodynamic favourability indicators (↓ΔH and ↓ΔG).

Performance indicator	EFB + N/A	EFB + DOL	EFB + OLI	PKS + N/A	PKS + DOL	PKS + OLI	SD + N/A	SD + DOL	SD + OLI	RH + N/A	RH + DOL	RH + OLI	CS + N/A	CS + DOL	CS + OLI
↓ ΔH	2	8	7	15	12	11	9	4	6	1	5	10	14	13	3
↓ ΔG	12	10	11	2	1	3	4	6	5	7	9	13	15	14	8
Total marks	14	18	18	17	13	14	13	10	11	8	14	23	29	27	11
Ranking	7th	4th	5th	6th	10th	8th	11th	14th	12th	15th	9th	3rd	1st	2nd	13th

↑: favorable in high value.
↓: favorable in low value.
The higher mark is given to the higher favorability, from 15 to 1.
N/A: without catalyst.
+DOL: with dolomite catalyst.
+OLI: with olivine catalyst.

biomass feedstocks. For CS, dolomite provided minimal improvement in energy requirements (ΔH), while olivine increases energy demand, making it less effective. For EFB, dolomite significantly reduces ΔH, outperforming olivine, whereas for RH, olivine showed a significant reduction in ΔH, making it more effective than dolomite. In contrast, neither catalyst improves the thermodynamic properties of PKS and SD, as both increase ΔH values compared to their raw forms. These results emphasize the importance of aligning catalyst selection with the specific feedstock to optimize gasification performance.

4. Conclusions

This study systematically ranked five Malaysian agricultural and industrial biomasses: empty fruit bunches (EFB) *Elaeis Guineensis*, palm kernel shell (PKS) (*Elaeis Guineensis)*, sawdust (SD) (*Neobalanocarpus Heimii, Hevea Brasiliensis, Tectona Grandis)*, rice husk (RH) (*Oryza Sativa)*, and coconut shell (CS) (*Cocos Nucifera)*, based on physicochemical characteristics, kinetic parameters, thermodynamic behavior, and catalytic effects via CO_2 gasification. The critical factors influencing the CO_2 gasification process include high fixed carbon, low ash content, high levels of carbon and hydrogen, significant cellulose/hemicellulose content, abundant alkali and alkaline earth metals, and low crystallinity. Overall, EFB emerged as the most favorable feedstock for CO_2 gasification, with the ranking sequence: EFB > PKS > CS > SD > RH, due to its balanced composition, i.e., high volatile matter (74.92 wt%), low ash (4.14 wt%), and optimal cellulose/hemicellulose content, coupled with moderate favorable kinetic (moderate activation energy in Stage II) and thermodynamic (moderate ΔH and ΔG) properties, contributed to the top ranking. CO_2 gasification proceeded via two stages: pyrolysis (Stage I, below 380 °C) and char gasification (Stage II, after 380 °C). Catalysts (dolomite and olivine) significantly reduced activation energy Ea in Stage II, particularly for EFB (from 131.84 to 112.88 kJ/mol with dolomite) and RH (from 168.86 to 103.37 kJ/mol with olivine), accelerating char conversion. Thermodynamically, lower enthalpy (ΔH) (found in PKS biomass) reduces energy requirements. Dolomite was effective in the case of EFB, while olivine was effective for RH. Future work will focus on the lab and higher-scale CO_2-biomass gasification in a fixed-bed reactor with and without a catalyst. Further, gas analysis produced during the gasification will be considered in the future scope of study.

CRediT authorship contribution statement

Zi Wei Ng: Writing – original draft, Visualization, Validation, Methodology, Investigation, Formal analysis, Data curation, Conceptualization. **Arshad Adam Salema:** Writing – review & editing, Supervision, Resources, Project administration, Methodology, Investigation, Funding acquisition, Formal analysis, Data curation, Conceptualization. **Izzudin Ibrahim:** Writing – review & editing, Validation, Supervision, Methodology, Investigation, Formal analysis, Data curation. **Hazratul Mumtaz Lahuri:** Writing – review & editing, Supervision, Methodology, Investigation, Conceptualization. **Yi Herng Chan:** Writing – review & editing, Supervision, Methodology, Investigation, Conceptualization.

Declaration of generative AI in scientific writing

Generative AI and AI-assisted technologies were used in the writing process to improve the readability and language of the manuscript.

Declaration of competing interest

The authors declare that they have no known competing financial interests or personal relationships that could have appeared to influence the work reported in this paper.

Acknowledgements

This work was financially supported by the PETRONAS Research Sdn. Bhd. (PRSB) [P-M010-CNI-000131]. Zi Wei Ng is grateful to Monash University Malaysia for Graduate Research support during her candidature.

Data availability

Data will be made available on request.

References

[1] PETRONAS, Sustainability- Delivering Net Zero, 2025.
[2] Y. Chantanumat, W. Phetwarotai, S. Sangthong, A. Palamanit, M.S. Abu Bakar, B. Cheirsilp, N. Phusunti, Characterization of bio-oil and biochar from slow pyrolysis of oil palm plantation and palm oil mill wastes, Biomass Convers. Biorefin. (2022) 1–13, https://doi.org/10.1007/s13399-021-02291-2.
[3] Ministry of Plantation and Commodities. Estimated Biomass Quantities, Current utilisation & findings, in: National Biomass Action Plan 2023- 2030, Ministry of Plantation and Commodities (KPK), Putrajaya, Malaysia, 2023, pp. 17–49.
[4] M.A. Sukiran, F. Abnisa, S. Syafiie, W.M.A. Wan Daud, A.B. Nasrin, A. Abdul Aziz, S.K. Loh, Experimental and modelling study of the torrefaction of empty fruit bunches as a potential fuel for palm oil mill boilers, Biomass Bioenergy 136 (2020) 105530, https://doi.org/10.1016/j.biombioe.2020.105530.
[5] A.L. Murmu, A. Patel, Towards sustainable bricks production: an overview, Constr Build Mater. 165 (2018) 112–125, https://doi.org/10.1016/j.conbuildmat.2018.01.038.
[6] J. Saravanan, P.V. Rao, Past investigations on development of sustainable bricks – a comprehensive review, Sustain. Chem. Environ. 3 (2023) 100030, https://doi.org/10.1016/j.scenv.2023.100030.
[7] M.N. Azit, R.K. Ahmad, S.A. Sulaiman, Environment friendly production of coconut shell charcoal through pyrolysis, in: Energy and Environment in the Tropics, Springer, 2022, pp. 245–261.
[8] R. Raj, J.V. Tirkey, P. Jena, Gasification of Briquette, Mahua wood, and Coconut shell and application to CI engines: comparative performance and optimisation analysis, Ind. Crops Prod. 199 (2023) 116758, https://doi.org/10.1016/j.indcrop.2023.116758.
[9] N. Linh Vu, N.D. Nguyen, T.M. Thanh Dinh, H.N. Nguyen, Cascading use of macadamia nutshell for production of energy and adsorbents through biomass gasification, Ind. Crops Prod. 206 (2023) 117662, https://doi.org/10.1016/j.indcrop.2023.117662.

[10] S. Valin, L. Bedel, J. Guillaudeau, S. Thiery, S. Ravel, CO_2 as a substitute of steam or inert transport gas in a fluidised bed for biomass gasification, Fuel 177 (2016) 288–295, https://doi.org/10.1016/j.fuel.2016.03.020.
[11] A. Prabhakar, A.K. Sadhukhan, P. Gupta, Kinetics and thermodynamics study of coal char gasification in CO_2 ambience, Int. J. Coal Preparation Utiliz. (2025) 1–14.
[12] Y. Wang, Z. Ge, F. Shang, C. Zhou, S. Guo, C. Ren, Kinetic analysis of CO_2 gasification of corn straw, Renew. Energy 203 (2023) 219–227, https://doi.org/10.1016/j.renene.2022.12.074.
[13] T.R. Pacioni, D. Soares, M. Di Domenico, J.L.F. Alves, E. Virmond, R.d.F.P. M. Moreira, H.J. José, Kinetic modeling of CO_2 gasification of biochars prepared from Brazilian agro-industrial residues: effect of biomass indigenous mineral content, Biomass Convers. Biorefin. 13 (2023) 6675–6688, https://doi.org/10.1007/s13399-021-01671-y.
[14] C.B. Felix, W.-H. Chen, A.T. Ubando, Y.-K. Park, K.-Y.A. Lin, A. Pugazhendhi, et al., A comprehensive review of thermogravimetric analysis in lignocellulosic and algal biomass gasification, Chem. Eng. J. 445 (2022) 136730, https://doi.org/10.1016/j.cej.2022.136730.
[15] S. Yousef, J. Eimontas, N. Striūgas, M.A. Abdelnaby, Pyrolysis and gasification kinetic behavior of mango seed shells using TG-FTIR-GC–MS system under N2 and CO_2 atmospheres, Renew. Energy 173 (2021) 733–749, https://doi.org/10.1016/j.renene.2021.04.034.
[16] C. Ma, Y. Yu, C. Tan, J. Hu, H. Wang, Kinetics, reaction mechanism and product distribution of lignocellulosic biomass pyrolysis using triple-parallel reaction model, combined kinetics, Py-GC/MS, and artificial neural networks, Ind. Crops Prod. 224 (2025) 120308, https://doi.org/10.1016/j.indcrop.2024.120308.
[17] M.W. Islam, A review of dolomite catalyst for biomass gasification tar removal, Fuel 267 (2020) 117095.
[18] G. Li, G.J. Nathan, M. Kuba, P.J. Ashman, W.L. Saw, Calcite or kaolinite addition for mitigating bed agglomeration during combustion and steam gasification of potassium-rich agricultural residues with olivine as the bed material, Energy Fuel. 36 (2022) 14267–14280, https://doi.org/10.1021/acs.energyfuels.2c02326.
[19] M.R. Sturgeon, M.H. O'Brien, P.N. Ciesielski, R. Katahira, J.S. Kruger, S.C. Chmely, et al., Lignin depolymerisation by nickel supported layered-double hydroxide catalysts, Green Chem. 16 (2014) 824–835, https://doi.org/10.1039/C3GC42138D.
[20] M. Mayoral, M. Izquierdo, J. Andrés, B. Rubio, Different approaches to proximate analysis by thermogravimetry analysis, Thermochim. Acta 370 (2001) 91–97, https://doi.org/10.1016/S0040-6031(00)00789-9.
[21] L.D. Torquato, P.M. Crnkovic, C.A. Ribeiro, M.S. Crespi, New approach for proximate analysis by thermogravimetry using CO 2 atmosphere: validation and application to different biomasses, J. Therm. Anal. Calorim. 128 (2017) 1–14, https://doi.org/10.1007/s10973-016-5882-z.
[22] ASTM E1131–20, Standard Test Method for Compositional Analysis by Thermogravimetry, 2020.
[23] ASTM D5865, A Standard Test Method for Gross Calorific Value of Coal and Coke, 2007.
[24] ASTM D5373-16, Standard Test Methods for Determination of Carbon, Hydrogen and Nitrogen in Analysis Samples of Coal and Carbon in Analysis Samples of Coal and Coke, 2016.
[25] A. Sluiter, B. Hames, R. Ruiz, C. Scarlata, J. Sluiter, D. Templeton, D. Crocker, Determination of structural carbohydrates and lignin in biomass, Laboratory Anal. Proc. 1617 (2008) 1–16.
[26] ASTM E572-13, Standard Test Method for Analysis of Stainless and Alloy Steels by Wavelength Dispersive X-Ray Fluorescence Spectrometry, 2016.
[27] A. Thygesen, J. Oddershede, H. Lilholt, A.B. Thomsen, K. Ståhl, On the determination of crystallinity and cellulose content in plant fibres, Cellulose 12 (2005) 563–576, https://doi.org/10.1007/s10570-005-9001-8.
[28] P. Bansal, M. Hall, M.J. Realff, J.H. Lee, A.S. Bommarius, Multivariate statistical analysis of X-ray data from cellulose: a new method to determine degree of crystallinity and predict hydrolysis rates, Bioresour. Technol. 101 (2010) 4461–4471, https://doi.org/10.1016/j.biortech.2010.01.068.
[29] F. Xu, Y.-C. Shi, D. Wang, X-ray scattering studies of lignocellulosic biomass: a review, Carbohydr. Polym. 94 (2013) 904–917, https://doi.org/10.1016/j.carbpol.2013.02.008.
[30] Y.D. Singh, P. Mahanta, U. Bora, Comprehensive characterization of lignocellulosic biomass through proximate, ultimate and compositional analysis for bioenergy production, Renew. Energy 103 (2017) 490–500, https://doi.org/10.1016/j.renene.2016.11.039.
[31] L. Segal, J.J. Creely, A. Martin Jr., C. Conrad, An empirical method for estimating the degree of crystallinity of native cellulose using the X-ray diffractometer, Textil. Res. J. 29 (1959) 786–794, https://doi.org/10.1177/004051755902901003.
[32] A. Fernandez, J. Soria, R. Rodriguez, J. Baeyens, G. Mazza, Macro-TGA steam-assisted gasification of lignocellulosic wastes, J. Environ. Manag. 233 (2019) 626–635, https://doi.org/10.1016/j.jenvman.2018.12.087.
[33] A.C.M. Loy, D.K.W. Gan, S. Yusup, B.L.F. Chin, M.K. Lam, M. Shahbaz, et al., Thermogravimetric kinetic modelling of in-situ catalytic pyrolytic conversion of rice husk to bioenergy using rice hull ash catalyst, Bioresour. Technol. 261 (2018) 213–222, https://doi.org/10.1016/j.biortech.2018.04.020.
[34] J.L.F. Alves, J.C.G. da Silva, V.F. da Silva Filho, R.F. Alves, W.V. de Araujo Galdino, R.F. De Sena, Kinetics and thermodynamics parameters evaluation of pyrolysis of invasive aquatic macrophytes to determine their bioenergy potentials, Biomass Bioenergy 121 (2019) 28–40, https://doi.org/10.1016/j.biombioe.2018.12.015.
[35] S. Vyazovkin, A.K. Burnham, L. Favergeon, N. Koga, E. Moukhina, L.A. Pérez-Maqueda, N. Sbirrazzuoli, ICTAC kinetics committee recommendations for analysis of multi-step kinetics, Thermochim. Acta 689 (2020) 178597, https://doi.org/10.1016/j.tca.2020.178597.
[36] D. Rammohan, N. Kishore, R.V.S. Uppaluri, Reaction kinetics and thermodynamic analysis of non-isothermal co-pyrolysis of Delonix regia and tube waste, Bioresour. Technol. Rep. 18 (2022) 101032, https://doi.org/10.1016/j.biteb.2022.101032.
[37] A. Fernandez, L.R. Ortiz, D. Asensio, R. Rodriguez, G. Mazza, Kinetic analysis and thermodynamics properties of air/steam gasification of agricultural waste, J. Environ. Chem. Eng. 8 (2020) 103829, https://doi.org/10.1016/j.jece.2020.103829.
[38] E. Kethobile, C. Ketlogetswe, J. Gandure, Torrefaction of non - oil Jatropha curcas L. (Jatropha) biomass for solid fuel, Heliyon 6 (2020) e05657, https://doi.org/10.1016/j.heliyon.2020.e05657.
[39] N.A. Samiran, M.N.M. Jaafar, J.-H. Ng, S.S. Lam, C.T. Chong, Progress in biomass gasification technique – with focus on Malaysian palm biomass for syngas production, Renew. Sustain. Energy Rev. 62 (2016) 1047–1062, https://doi.org/10.1016/j.rser.2016.04.049.
[40] M. Mierzwa-Hersztek, K. Gondek, M. Jewiarz, K. Dziedzic, Assessment of energy parameters of biomass and biochars, leachability of heavy metals and phytotoxicity of their ashes, J. Mater. Cycles Waste Manag. 21 (2019) 786–800, https://doi.org/10.1007/s10163-019-00832-6.
[41] Y. Gao, M. Wang, A. Raheem, F. Wang, J. Wei, D. Xu, et al., Syngas production from biomass gasification: influences of feedstock properties, reactor type, and reaction parameters, ACS Omega 8 (2023) 31620–31631, https://doi.org/10.1021/acsomega.3c03050.
[42] A.A. Salema, F.N. Ani, Pyrolysis of oil palm empty fruit bunch biomass pellets using multimode microwave irradiation, Bioresour. Technol. 125 (2012) 102–107, https://doi.org/10.1016/j.biortech.2012.08.002.
[43] S.-J. Kim, S.-H. Jung, J.-S. Kim, Fast pyrolysis of palm kernel shells: influence of operation parameters on the bio-oil yield and the yield of phenol and phenolic compounds, Bioresour. Technol. 101 (2010) 9294–9300, https://doi.org/10.1016/j.biortech.2010.06.110.
[44] Y. Zhao, S. Sun, H. Zhou, R. Sun, H. Tian, J. Luan, J. Qian, Experimental study on sawdust air gasification in an entrained-flow reactor, Fuel Process. Technol. 91 (2010) 910–914, https://doi.org/10.1016/j.fuproc.2010.01.012.
[45] R. Krishnan, L. Hauchhum, R. Gupta, S. Pattanayak, Prediction of equations for higher heating values of biomass using proximate and ultimate analysis, in: 2018 2nd International Conference on Power, Energy and Environment: towards Smart Technology (ICEPE), IEEE, 2018, pp. 1–5, https://doi.org/10.1109/EPETSG.2018.8658984.
[46] P. Lahijani, Z.A. Zainal, A.R. Mohamed, M. Mohammadi, CO_2 gasification reactivity of biomass char: catalytic influence of alkali, alkaline earth and transition metal salts, Bioresour. Technol. 144 (2013) 288–295, https://doi.org/10.1016/j.biortech.2013.06.059.
[47] A.A. Siyal, L. Yang, B. Ali, M. Hassan, C. Zhou, X. Li, et al., Characterization and quality analysis of biomass pellets prepared from furfural residue, sawdust, corn stalk and sewage sludge, Fuel Process. Technol. 241 (2023) 107620, https://doi.org/10.1016/j.fuproc.2022.107620.
[48] J. Manu, T.G. Kailas, V. Madav, Exploring the synergetic effects of rice husk, cashew shell, and cashew husk biomass blends on fluidized bed gasification for enhanced hydrogen production, J. Clean. Prod. 419 (2023) 137991, https://doi.org/10.1016/j.jclepro.2023.137991.
[49] G.L. Manga, A.M. Abioyec, J. Mohammed, M. Markus, Characterization of oil palm empty fruit bunch and coconut shell for the production of fuel briquettes, Int. J. Appl. Technol. Res. 4 (2023) 8–16, https://doi.org/10.35313/ijatr.v4i1.119.
[50] A. Özyuğuran, S. Yaman, Prediction of calorific value of biomass from proximate analysis, Energy Proc. 107 (2017) 130–136, https://doi.org/10.1016/j.egypro.2016.12.149.
[51] P. Lahijani, Z.A. Zainal, A.R. Mohamed, M. Mohammadi, Ash of palm empty fruit bunch as a natural catalyst for promoting the CO_2 gasification reactivity of biomass char, Bioresour. Technol. 132 (2013) 351–355, https://doi.org/10.1016/j.biortech.2012.10.092.
[52] C. Wu, Z. Wang, J. Huang, P.T. Williams, Pyrolysis/gasification of cellulose, hemicellulose and lignin for hydrogen production in the presence of various nickel-based catalysts, Fuel 106 (2013) 697–706, https://doi.org/10.1016/j.fuel.2012.10.064.
[53] J.D. Coral Medina, A.L. Woiciechowski, A.Z. Filho, S.K. Brar, A.I. Magalhães Júnior, C.R. Soccol, Energetic and economic analysis of ethanol, xylitol and lignin production using oil palm empty fruit bunches from a Brazilian factory, J. Clean. Prod. 195 (2018) 44–55, https://doi.org/10.1016/j.jclepro.2018.05.189.
[54] M.A. Sukiran, F. Abnisa, W.M.A. Wan Daud, N. Abu Bakar, S.K. Loh, A review of torrefaction of oil palm solid wastes for biofuel production, Energy Convers. Manag. 149 (2017) 101–120, https://doi.org/10.1016/j.enconman.2017.07.011.
[55] D. Tavares, M. Cavali, V.D. Tanobe, L.A. Torres, A.S. Rozendo, A. Zandoná Filho, et al., Lignin from residual sawdust of Eucalyptus spp.—Isolation, characterization, and evaluation of the antioxidant properties, Biomass (2022) 195–208, https://doi.org/10.3390/biomass2030013.
[56] M. Shahabazuddin, T. Sarat Chandra, S. Meena, R.K. Sukumaran, N.P. Shetty, S. N. Mudliar, Thermal assisted alkaline pretreatment of rice husk for enhanced biomass deconstruction and enzymatic saccharification: Physico-chemical and structural characterization, Bioresour. Technol. 263 (2018) 199–206, https://doi.org/10.1016/j.biortech.2018.04.027.
[57] S.N.I.H.A. Nadzri, M.T.H. Sultan, A.U.M. Shah, S.N.A. Safri, A.R.A. Talib, M. Jawaid, A.A. Basri, A comprehensive review of coconut shell powder composites: preparation, processing, and characterization, J. Thermoplast. Compos. Mater. 35 (2022) 2641–2664, https://doi.org/10.1177/0892705720930808.

[58] M.J. Taherzadeh, K. Karimi, Pretreatment of lignocellulosic wastes to improve ethanol and biogas production: a review, Int. J. Mol. Sci. 9 (2008) 1621–1651, https://doi.org/10.3390/ijms9091621.
[59] F.A. Razmi, N. Ngadi, S. Wong, I.M. Inuwa, L.A. Opotu, Kinetics, thermodynamics, isotherm and regeneration analysis of chitosan modified pandan adsorbent, J. Clean. Prod. 231 (2019) 98–109, https://doi.org/10.1016/j.jclepro.2019.05.228.
[60] S. Periyasamy, P. Manivasakan, C. Jeyaprabha, S. Meenakshi, N. Viswanathan, Fabrication of nano-graphene oxide assisted hydrotalcite/chitosan biocomposite: an efficient adsorbent for chromium removal from water, Int. J. Biol. Macromol. 132 (2019) 1068–1078, https://doi.org/10.1016/j.ijbiomac.2019.03.232.
[61] E. Babiker, M.A. Al-Ghouti, N. Zouari, G. McKay, Removal of boron from water using adsorbents derived from waste tire rubber, J. Environ. Chem. Eng. 7 (2019) 102948, https://doi.org/10.1016/j.jece.2019.102948.
[62] S. Wong, Y. Lee, N. Ngadi, I.M. Inuwa, N.B. Mohamed, Synthesis of activated carbon from spent tea leaves for aspirin removal, Chin. J. Chem. Eng. 26 (2018) 1003–1011, https://doi.org/10.1016/j.cjche.2017.11.004.
[63] A. Gupta, S.K. Thengane, S. Mahajani, CO_2 gasification of char from lignocellulosic garden waste: experimental and kinetic study, Bioresour. Technol. 263 (2018) 180–191, https://doi.org/10.1016/j.biortech.2018.04.097.
[64] V.A. Belyi, E.V. Udoratina, A.V. Kuchin, Kinetics of the thermocatalytic conversion of lignocellulose, Kinet. Catal. 56 (2015) 663–669, https://doi.org/10.1134/S002315841505002X.
[65] Y. Huang, X. Yin, C. Wu, C. Wang, J. Xie, Z. Zhou, et al., Effects of metal catalysts on CO_2 gasification reactivity of biomass char, Biotechnol. Adv. 27 (2009) 568–572, https://doi.org/10.1016/j.biotechadv.2009.04.013.
[66] M. Perander, N. DeMartini, A. Brink, J. Kramb, O. Karlström, J. Hemming, et al., Catalytic effect of Ca and K on CO_2 gasification of spruce wood char, Fuel 150 (2015) 464–472, https://doi.org/10.1016/j.fuel.2015.02.062.
[67] R.K. Ahmad, S.A. Sulaiman, S. Yusup, S.S. Dol, M. Inayat, H.A. Umar, Exploring the potential of coconut shell biomass for charcoal production, Ain Shams Eng. J. 13 (2022) 101499, https://doi.org/10.1016/j.asej.2021.05.013.
[68] S. Novianti, A. Nurdiawati, I.N. Zaini, P. Prawisudha, H. Sumida, K. Yoshikawa, Low-potassium fuel production from empty fruit bunches by hydrothermal treatment processing and water leaching, Energy Proc. 75 (2015) 584–589, https://doi.org/10.1016/j.egypro.2015.07.460.
[69] S. Sohni, N.A.N. Norulaini, R. Hashim, S.B. Khan, W. Fadhullah, A.K. Mohd Omar, Physicochemical characterization of Malaysian crop and agro-industrial biomass residues as renewable energy resources, Ind. Crops Prod. 111 (2018) 642–650, https://doi.org/10.1016/j.indcrop.2017.11.031.
[70] M. Hussain, L.D. Tufa, S. Yusup, H. Zabiri, Thermochemical behavior and characterization of palm kernel shell via TGA/DTG technique, Mater. Today Proc. 16 (2019) 1901–1908, https://doi.org/10.1016/j.matpr.2019.06.067.
[71] P.P. Ikubanni, M. Oki, A.A. Adeleke, A.A. Adediran, O.S. Adesina, Influence of temperature on the chemical compositions and microstructural changes of ash formed from palm kernel shell, Results Eng. 8 (2020) 100173, https://doi.org/10.1016/j.rineng.2020.100173.
[72] C. Liao, C. Wu, Y. Yan, The characteristics of inorganic elements in ashes from a 1 MW CFB biomass gasification power generation plant, Fuel Process. Technol. 88 (2007) 149–156, https://doi.org/10.1016/j.fuproc.2005.06.008.
[73] C. Hanping, L. Bin, Y. Haiping, Y. Guolai, Z. Shihong, Experimental investigation of biomass gasification in a fluidized bed reactor, Energy Fuel. 22 (2008) 3493–3498, https://doi.org/10.1021/ef800180e.
[74] P. Lahijani, Z.A. Zainal, Gasification of palm empty fruit bunch in a bubbling fluidized bed: a performance and agglomeration study, Bioresour. Technol. 102 (2011) 2068–2076, https://doi.org/10.1016/j.biortech.2010.09.101.
[75] M. Mohammed, A. Salmiaton, W.W. Azlina, M.M. Amran, Gasification of oil palm empty fruit bunches: a characterization and kinetic study, Bioresour. Technol. 110 (2012) 628–636, https://doi.org/10.1016/j.biortech.2012.01.056.
[76] X. Chen, Y. Zhang, J. Mei, G. Zhao, Q. Lyu, X. Lyu, et al., Ball milling for cellulose depolymerization and alcoholysis to produce methyl levulinate at mild temperature, Fuel Process. Technol. 188 (2019) 129–136, https://doi.org/10.1016/j.fuproc.2019.02.002.
[77] M. Kumar, S.N. Upadhyay, P.K. Mishra, A comparative study of thermochemical characteristics of lignocellulosic biomasses, Bioresour. Technol. Rep. 8 (2019) 100186, https://doi.org/10.1016/j.biteb.2019.100186.
[78] A. Hideno, Comparison of the thermal degradation properties of crystalline and amorphous cellulose, as well as treated lignocellulosic biomass, Bioresources 11 (2016) 6309–6319, https://doi.org/10.15376/biores.11.3.6309-6319.
[79] A. Meng, S. Chen, Y. Long, H. Zhou, Y. Zhang, Q. Li, Pyrolysis and gasification of typical components in wastes with macro-TGA, Waste Manag. 46 (2015) 247–256, https://doi.org/10.1016/j.wasman.2015.08.025.
[80] M. Nasfi, M. Carrier, S. Salvador, Kinetic modelling of biomass fast devolatilization using Py-MS: model-free and model-based approaches, J. Anal. Appl. Pyrolysis 174 (2023) 106128, https://doi.org/10.1016/j.jaap.2023.106128.
[81] S.B. Prajapati, A. Gautam, S. Gautam, Non-isothermal kinetic study by TGA analysis of printed circuit boards and cotton stalk, Biomass Bioenergy 172 (2023) 106746, https://doi.org/10.1016/j.biombioe.2023.106746.
[82] M. Bhattacharyya, K.P. Shadangi, P. Mahanta, K. Mohanty, Co-pyrolysis of coal-biomass: study on reaction kinetics and thermodynamics, Biofuel Bioprod. Biorefining 16 (2022) 725–742, https://doi.org/10.1002/bbb.2333.
[83] A. Kumar, S.N. Reddy, Study the catalytic effect on pyrolytic behavior, thermal kinetic and thermodynamic parameters of Ni/Ru/Fe-impregnated sugarcane bagasse via thermogravimetric analysis, Ind. Crops Prod. 178 (2022) 114564, https://doi.org/10.1016/j.indcrop.2022.114564.
[84] H. Yu, G. Chen, Y. Xu, D. Chen, Experimental study on the gasification characteristics of biomass with CO_2/air in an entrained-flow gasifier, Bioresources 11 (2016) 6085–6096, https://doi.org/10.15376/biores.11.3.6085-6096.
[85] V.M. Kislov, S.V. Glazov, E.A. Salgansky, Y.Y. Kolesnikova, M.V. Salganskaya, Coal gasification by a mixture of air and carbon dioxide in the filtration combustion mode, Combust. Explos. Shock Waves 52 (2016) 320–325, https://doi.org/10.1134/S0010508216030102.
[86] B.B. Nyakuma, S. Wong, O. Oladokun, Non-oxidative thermal decomposition of oil palm empty fruit bunch pellets: fuel characterisation, thermogravimetric, kinetic, and thermodynamic analyses, Biomass Convers. Biorefin. 11 (2021) 1273–1292, https://doi.org/10.1007/s13399-019-00568-1.
[87] A.L.K. Chee, B.L.F. Chin, S.M.X. Goh, Y.H. Chai, A.C.M. Loy, K.W. Cheah, et al., Thermo-catalytic co-pyrolysis of palm kernel shell and plastic waste mixtures using bifunctional HZSM-5/limestone catalyst: kinetic and thermodynamic insights, J. Energy Inst. 107 (2023) 101194, https://doi.org/10.1016/j.joei.2023.101194.
[88] N. Agnihotri, G.K. Gupta, M.K. Mondal, Thermo-kinetic analysis, thermodynamic parameters and comprehensive pyrolysis index of Melia azedarach sawdust as a genesis of bioenergy, Biomass Convers. Biorefin. 14 (2024) 1863–1880, https://doi.org/10.1007/s13399-022-02524-y.
[89] M. Kumar, P.K. Mishra, S.N. Upadhyay, Thermal degradation of rice husk: effect of pre-treatment on kinetic and thermodynamic parameters, Fuel 268 (2020) 117164, https://doi.org/10.1016/j.fuel.2020.117164.
[90] L. Addagada, A.M. Nair, Assessment of kinetics and thermodynamic parameters of Cocos Nucifera using thermogravimetric analysis, Biomass Convers. Biorefin. (2024), https://doi.org/10.1007/s13399-024-05962-y.
[91] Y. Xu, B. Chen, Investigation of thermodynamic parameters in the pyrolysis conversion of biomass and manure to biochars using thermogravimetric analysis, Bioresour. Technol. 146 (2013) 485–493, https://doi.org/10.1016/j.biortech.2013.07.086.
[92] C. Wu, S. Ge, J. Li, B. Shi, Y. Wang, S. Wang, F. Zhou, The effect of $N2/CO_2$ blend ratios on the pyrolysis and combustion behaviors of coal particles: kinetic and thermodynamic analyses, J. Loss Prev. Process. Ind. 84 (2023) 105120, https://doi.org/10.1016/j.jlp.2023.105120.
[93] M. Tangarfa, M. El Hazzat, S. Sebbahi, F. Kifani-Sahban, A. El Hamidi, Unravelling the kinetics and thermodynamics of CO_2 gasification of lignin char: an isoconversional and multi-methodological analysis, Emerg. Mater. (2024), https://doi.org/10.1007/s42247-024-00829-4.
[94] M. Baratieri, E. Pieratti, T. Nordgreen, M. Grigiante, Biomass gasification with dolomite as catalyst in a small fluidized bed experimental and modelling analysis, Waste Biomass Valori. 1 (2010) 283–291, https://doi.org/10.1007/s12649-010-9034-6.
[95] K. Wang, K.H. Kim, R.C. Brown, Catalytic pyrolysis of individual components of lignocellulosic biomass, Green Chem. 16 (2014) 727–735, https://doi.org/10.1039/C3GC41288A.
[96] E. Keszei, Catalysts and catalytic reactions, in: E. Keszei (Ed.), Reaction Kinetics: an Introduction, Springer International Publishing, Cham, 2021, pp. 133–159.
[97] S. Stendardo, L. Di Felice, K. Gallucci, P.U. Foscolo, CO_2 capture with calcined dolomite: the effect of sorbent particle size, Biomass Convers. Biorefin. 1 (2011) 149–161, https://doi.org/10.1007/s13399-011-0018-y.
[98] S. Rapagnà, G. Spinelli, Biomass gasification with dolomite and olivine particles as a bed inventory in presence of ceramic filters, Chem. Eng. Trans. 52 (2016) 289–294, https://doi.org/10.3303/CET1652049.